ELSEVIER

Journal of Structural Geology 28 (2006) 1536–1552

JOURNAL OF STRUCTURAL GEOLOGY

www.elsevier.com/locate/jsg

Insights into the post-emplacement history of the Saunstein granitic dyke showing heterogeneous deformation and inconsistent shear-sense indicators (Bavarian Forest, Germany)

E. Galadí-Enríquez [a,*], G. Zulauf [a], F. Heidelbach [b], J. Rohrmüller [c]

[a] *Geologisch-Paläontologisches Institut, Universität Frankfurt am Main, Senckenberganlage 32–34, D-60054 Frankfurt a. M., Germany*
[b] *Bayerisches Geoinstitut, Universität Bayreuth, D-95440 Bayreuth, Germany*
[c] *Bayerisches Landesamt fuer Umwelt, Leopoldstr. 30, D-95615 Marktredwitz, Germany*

Received 26 May 2005; received in revised form 26 April 2006; accepted 24 May 2006
Available online 7 July 2006

Abstract

The recent mapping survey undertaken in the Bavarian Forest led to the discovery of several E–W trending sinistral shear zones, usually affecting granitic dykes or areas intruded by dykes. We studied a granitic dyke affected by one of these shear zones. The deformation in the dyke, as well as in other dykes of the region, is not homogeneous and concentrates mainly next to the contact to the country rock. The differences in mineralogy between dyke and host probably controlled the distribution of strain, favoring the deformation of the lithology richer in quartz, i.e. the granite dyke, next to a rheological boundary, i.e. the contact to the host rock. As inferred from microfabrics and quartz textures, quartz deformation occurred by dislocation creep accommodated by grain boundary migration and subgrain rotation recrystallization. Intracrystalline glide on prism planes in the <*a*> direction indicate a temperature of ~500–550 °C. Only in the most strained, fine grained bands was deformation achieved by grain boundary sliding. A late shear-sense reversal after the principal sinistral deformation in the dyke led to the development of a dextral quartz shape fabric. This reflects on the one hand how quartz is able to record late, low-strain overprints, and on the other hand, how oblique quartz foliations may lead to wrong interpretations when being used without corroboration of other shear-sense indicators.

Keywords: Shear zone; Dyke; Mylonite; Quartz fabric; Oblique foliation; Bohemian Massif

1. Introduction

The Variscan belt of Europe is the result of a long period of convergence between Laurussia and Gondwana during the Paleozoic, involving collision of several microplates. Its evolution has been studied and partly reconstructed on the basis of plate tectonics (e.g. Franke, 1989a,b, 2000; Matte, 1986, 1991; Matte et al., 1990). The structure and tectonic evolution of the Bohemian Massif have been studied by several authors in different areas (e.g. Beer, 1981; Behrmann and Tanner, 1997; Brandmayr et al., 1995; Büttner and Kruhl, 1997; Fuchs, 1986; Scheuvens and Zulauf, 2000; Zulauf et al., 2002), sometimes paying special attention to the most prominent shear zones. Our study area is located in the southern part of the Bavarian Forest, which constitutes the south-western end of the Bohemian Massif (Fig. 1). Tectonic studies are scarce in this region and the few existing ones focus on the main tectonic directions visible in map view, i.e. those of the most important shear zones: the dextral NW–SE trending Bayerischer Pfahl shear zone and subsidiary or parallel ones. The German word ‘‘Pfahl’’ makes reference to the quartz lode formed during the late history of the shear zone. The Bayerischer Pfahl shear zone and associated shear zones

* Corresponding author. Tel.: +49 (0)9131 27536; fax: +49 (0)69 798 22958.
E-mail address: e.galadi@em.uni-frankfurt.de (E. Galadí-Enríquez).

0191-8141/$ - see front matter © 2006 Elsevier Ltd. All rights reserved.
doi:10.1016/j.jsg.2006.05.007

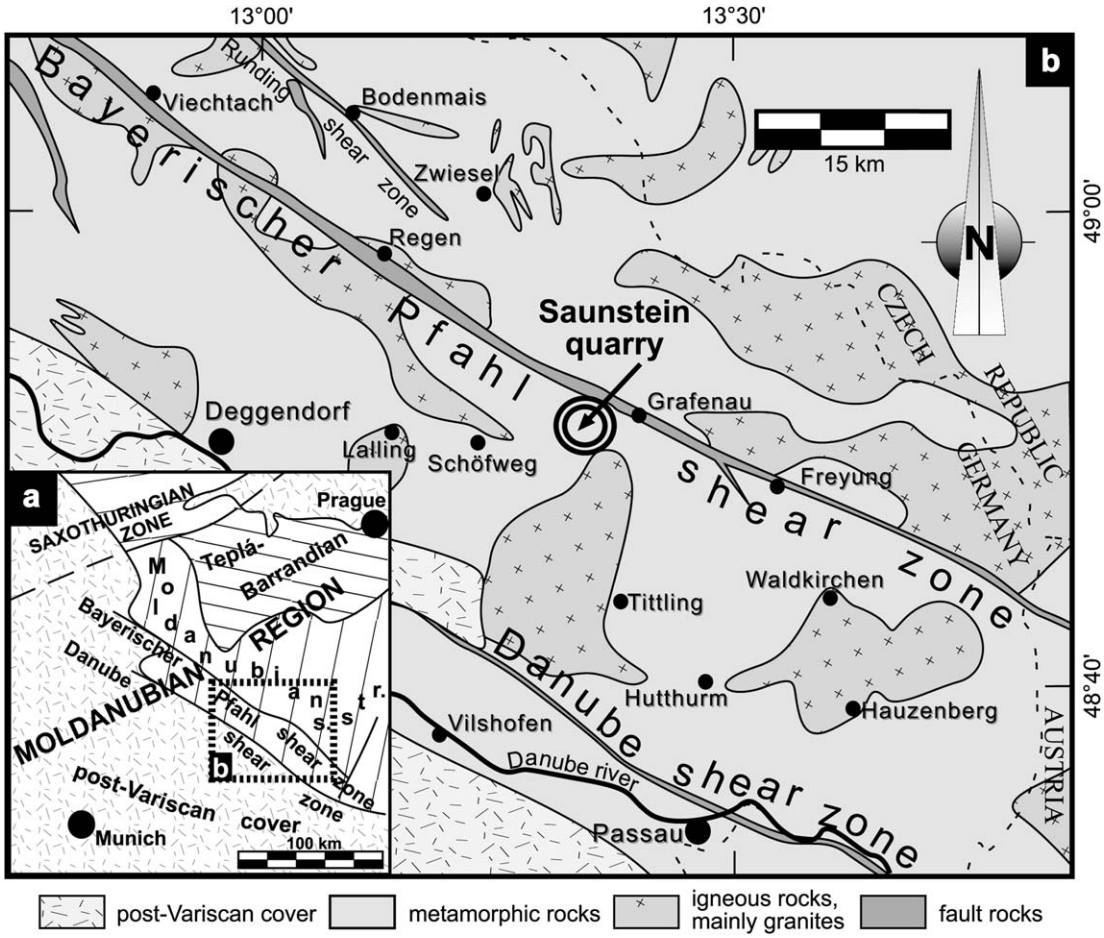

Fig. 1. (a) Geological map of the south-western Bohemian Massif. (b) Simplified geological map of the SE part of the Bavarian Forest. The position of the Saunstein quarry is indicated (coordinates N 48°51′26.2″ E 013°20′03.1″).

have been active over a wide time and temperature span ranging from amphibolite facies to near-surface conditions (Beer, 1981; Brandmayr et al., 1995; Hoffmann, 1962; Masch and Cetin, 1991) from pre-Variscan to Miocene times (Freudenberger, 1996, and references therein). Until the recent new mapping of some regions of the Bavarian Forest (Blaha, in press; Galadí-Enríquez, in press) the existence of sinistral, roughly E–W trending shear zones, usually affecting granitic dykes or areas intruded by dykes, was nearly unknown. The first aim of this study is therefore to analyze one of these newly discovered shear zones focusing on aspects such as fabrics, strain, stress and mass transfer. This analysis can provide some key information about: (i) the thermal conditions during sinistral shearing, (ii) the geometry of the deformation, (iii) the pre- or synkinematic character of the deformed dyke in relation to the sinistral movement, (iv) the causes for the concentration of E–W sinistral deformation in this dyke and similar ones and (v) the causes for the inhomogeneous deformation inside the dyke.

An interesting problem arises when trying to apply the traditionally defined shear-sense criteria (e.g. Bouchez et al., 1983; Simpson and Schmid, 1983; Hanmer and Passchier, 1991) to the deformed granite dyke. All indicators point to a sinistral shear sense, whereas the shape-preferred orientation of quartz grains (in the literature also called oblique foliation or shape fabric) shows the opposite. The second goal of this paper is to investigate this up to now poorly documented phenomenon, to shed some light on its origin and to reexamine the reliability of oblique foliations as a shear-sense indicator.

2. Geological setting

The present study focuses on a variably deformed granitic dyke cropping out in the Saunstein quarry, which is located in the southern Bavarian Forest (SE Germany). Geologically the quarry is situated in the Moldanubian Zone (Suess, 1903) of the Central European Variscides, between the NW–SE trending Bayerischer Pfahl and Danube shear zones, in the so-called Bavaricum (sensu Fuchs, 1976) or Bavarian Terrane (sensu Fiala et al., 1995). The most common rocks in the study area are migmatic gneisses affected by anatexis at different degrees and intruded by different kinds of igneous rocks pre- or post-dating the anatexis (Propach et al., 2000; Chen and Siebel, 2004; Siebel et al., 2005). This anatexis, and the associated high-*T*/low-*P* metamorphism, has been dated around 320–326 Ma in neighboring areas to the

Saunstein quarry (U-Pb on zircon, Kalt et al., 2000; U-Pb on monazite and zircon, Propach et al., 2000). In other parts of the Moldanubian Zone the age of the high-*T*/low-*P* metamorphism can range between 316 and 330 Ma (U-Th-Pb on zircon and monazite, Rb-Sr whole-rock and biotite, Grauert et al., 1974; U-Pb on monazite, Friedl et al., 1993; U-Pb on zircon, Teipel et al., 2004).

The migmatites in the Saunstein quarry were named "Palite" by Frentzel (1911). In recent papers (Blaha, in press; Galadí-Enríquez, in press) these rocks are considered to have been affected by Variscan anatexis. Consequently they are called dark-colored diatexites. A diatexite is a variety of migmatite where the darker and the lighter parts form schlieren and nebulitic structures which merge into one another (Wimmenauer and Bryhni, 2002). Siebel et al. (2005) consider dark-colored diatexites to have evolved from a plutonic protolith, which intruded at 334 ± 3 Ma. Dark-colored diatexites show a tectonic foliation which parallels the steeply dipping NW–SE striking mylonitic foliation of the Bayerischer Pfahl shear zone. The latter results from dextral simple shear (Beer, 1981; Wallbrecher et al., 1990; Masch and Cetin, 1991) and will be referred to in this manuscript as D2. The dark-colored diatexites of the Saunstein quarry are cut by a subvertical, E–W (N070E to N090E) trending granite dyke (Artmann, 2001). The dyke shows a mylonitic foliation trending subparallel to the contact to the host rock and a subhorizontal stretching lineation. This deformation will be referred to as D3 and is the central subject of our study. The dyke's emplacement age is 324.4 ± 0.8 Ma according to Galadí-Enríquez et al. (2005, U-Pb on monazite), 326 ± 9 Ma after Siebel et al. (2005, U-Pb on zircon) and 316 ± 6 Ma after Christinas et al. (1991, Rb-Sr on muscovite). Similar dykes cropping out in the study area are the object of current research.

3. Outcrop description and sampling mode

The Saunstein granite dyke is about 50 m thick, but only the northern half of it is well exposed in the quarry. The D3 mylonitic foliation and stretching lineation of the dyke are particularly well developed adjacent to the contact to the host rock and become gradually weaker towards the dyke centre (Figs. 2 and 3). The dyke was sampled at intervals from a few centimeters in highly deformed parts up to 2 meters in less deformed parts. *XZ* and *YZ* sections at hand specimen and thin section scale were prepared for structural analysis.

A detailed geologic profile along the eastern wall of the quarry allows the recognition of two more dykes north of the principal one (Fig. 2). One of them is 0.15 m thick and presents a very strong D3 mylonitic foliation. The other one is 0.5 m thick and is affected by D3 at the southern part and practically undeformed at the northern contact, where a not strongly marked but visibly chilled margin is present (Fig. 4). The internal characteristics of these two smaller dykes are similar to those of the principal dyke and will therefore not be the object of further studies. Nevertheless, there is an important fact accompanying these dykes: the host rock at their southern part is affected by D3. The host rock at the contact to the main dyke is also likely to have been affected by D3 (Fig. 2), but structures related to D3 cannot be unequivocally identified due to a late cataclastic overprint.

4. Methods

4.1. Optical microscopy

We studied several thin sections parallel to the *XZ* and *YZ* planes of the finite strain ellipsoid under the light microscope in order to (i) describe the microstructural features characterizing each deformation phase that affected the principal dyke and its host rock, (ii) estimate the temperature conditions and the deformation mechanisms governing each phase and (iii) study the changes in intensity and style of deformation inside the principal dyke.

4.2. Electron backscatter diffraction

The application of electron backscatter diffraction (e.g. Prior et al., 1999) to the study of quartz microfabrics provides information about the existence of lattice preferred orientation. This technique was applied using the equipment available at the Bayerisches Geoinstitut of the University of Bayreuth (Germany). From different granite and diatexite samples slabs parallel to the *XZ* sections of the finite strain ellipsoid were cut and polished in a first step up to a particle size of the medium of 1 μm and finally with a high pH silica solution (SYTON). The samples were coated with carbon up to a thickness of about 4 nm to reduce charging effects and scanned under an accelerating voltage of 30 keV. The beam current was about 4 nA. A rectangular area of the sample was delimited and scanned with a step width between 170 and 20 μm, depending on the grain size in every case.

4.3. Strain analysis

Four samples from the principal dyke were selected for the application of the R_f/Φ' method (Peach and Lisle, 1979; Ramsay and Huber, 1983). This method allows the calculation of the aspect ratio of the finite strain ellipse (R_s) from initially elliptical markers. As marker we used feldspar mantled porphyroclasts, whose initial form after crystallization from melt is comparable to an ellipse. Hand specimens were cut parallel to the *XZ* and *YZ* principal planes of the finite strain ellipsoid and scanned. For an average of 73 particles per section the elliptical shape of porphyroclasts (R_f) and the orientation of their major axis (Φ') were measured. Making use of the program "STRAIN" (Unzog, 1990), the strain ratios on the above mentioned principal planes ($R_{s,xz}$ and $R_{s,yz}$) were calculated. $R_{s,xy}$ was obtained from $R_{s,xz}/R_{s,yz}$.

The angle between *S* and *C* planes was used to calculate the strain in three of the former samples using the formula:

$$\gamma = 2/\tan 2\theta', \quad (1)$$

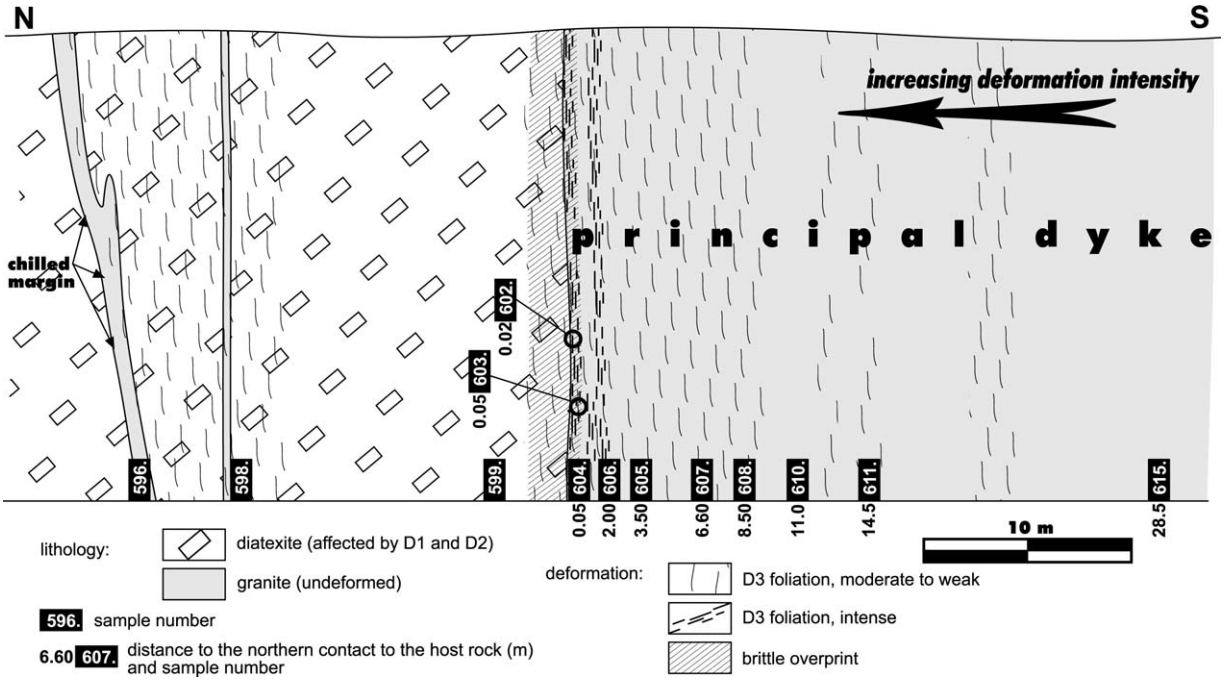

Fig. 2. Geological section along the eastern wall of the Saunstein quarry. The location of the samples used in this study is indicated.

where γ is the shear strain and θ' the angle between S and C (Ramsay and Graham, 1970).

4.4. X-ray fluorescence analysis

Six samples distributed throughout the principal dyke were selected to be analyzed by means of X-ray fluorescence (XRF) at the Bayerisches Landesamt fuer Umwelt (Marktredwitz, Germany). The results were used in the application of the isocon-diagram method and the Zr thermometry.

4.4.1. Isocon diagram

In order to check a possible mass transfer and volume change during deformation the isocon-diagram method (Grant, 1986) was applied. This method consists of plotting the concentration of components in an unaltered rock

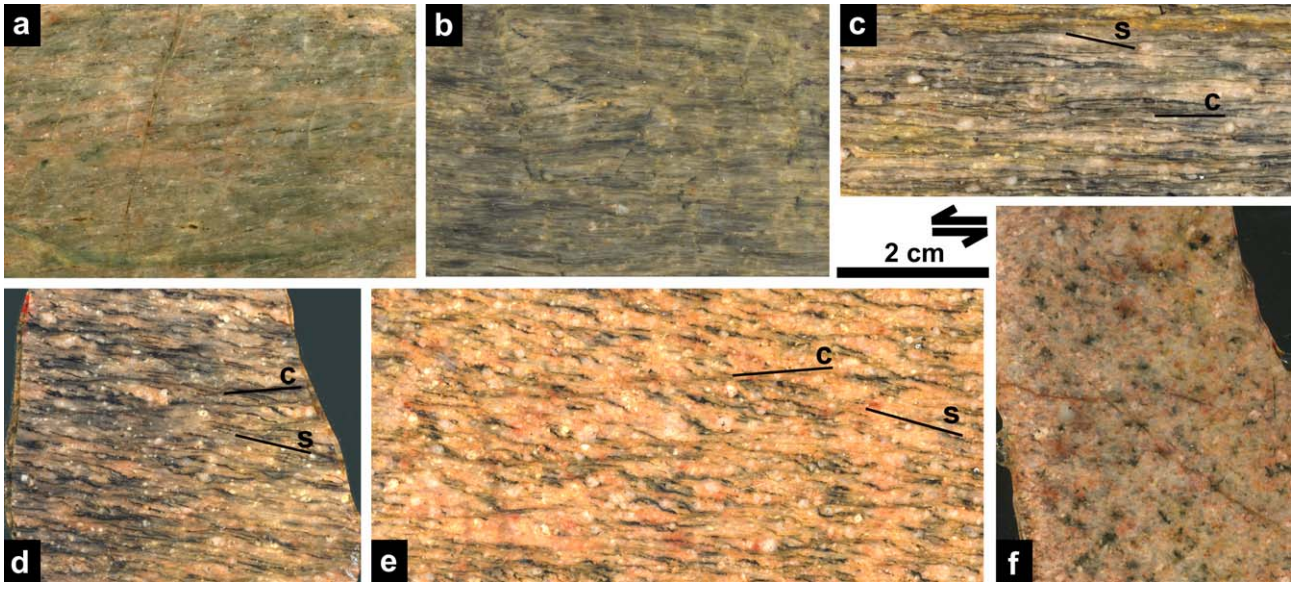

Fig. 3. Hand specimens of granite in order of increasing distance to the host rock and decreasing intensity of D3, *XZ* sections. (a) Sample 603, *S* and *C* surfaces are parallel to each other. (b) Sample 606, *S* and *C* surfaces are parallel to each other, an asymmetric fold is observable. (c) Sample 605, *S* and *C* surfaces at an angle of 12°. (d) Sample 607, *S* and *C* surfaces at an angle of 18°. (e) Sample 608, *S* and *C* surfaces at an angle of 20°. (f) Sample 615, nearly undeformed. This figure can be viewed in color in the online version of this article.

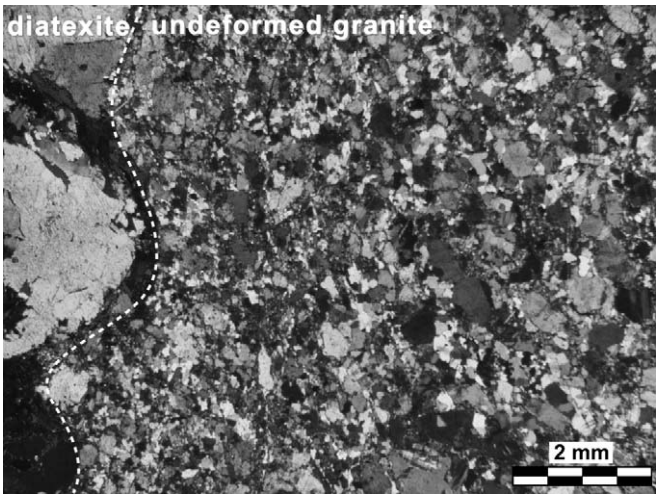

Fig. 4. Photomicrograph of sample 596 (see Fig. 2 for location), showing a decrease in grain size in undeformed granite towards the contact to the host rock. Crossed polarizers.

(undeformed in our case) against the concentration in an altered (deformed) equivalent. The equation linking the concentration of a component relative to its concentration prior to deformation is:

$$\frac{\Delta C_i}{C_i^{\mathrm{O}}} = \frac{M^{\mathrm{A}}}{M^{\mathrm{O}}} \times \frac{C_i^{\mathrm{A}}}{C_i^{\mathrm{O}}} - 1, \tag{2}$$

where C is the concentration and M is the mass of the sample. i, O and A represent a given component, the undeformed state and the deformed state respectively. If deformation carries no change in volume, both mobile and immobile components will plot on a line of slope = 1. If deformation was accompanied by mass loss, which normally takes place by removing the mobile components, then the immobile components would become more concentrated and tend to plot on a line of slope >1.

4.4.2. Zr thermometry

From the zirconium content of the samples, the temperature of the granitic melt can be calculated after Watson and Harrison's (1983) zircon solubility model making use of the equation:

$$D = \frac{-3.80 - 0.85(M-1) + 12900}{T}, \tag{3}$$

where D represents the solubility of zircon in the melt, T the temperature and M the cation ratio

$$M = \frac{\mathrm{Na} + \mathrm{K} + 2\mathrm{Ca}}{\mathrm{Al} \times \mathrm{Si}}. \tag{4}$$

4.5. Electron microprobe analysis

Electron microprobe analyses of feldspars were performed with the aim of studying variations in chemical composition between old and newly crystallized feldspar grains. The analyses were performed at the Institut für Geologie und Mineralogie, Erlangen-Nuernberg University (Germany), using a JEOL Superprobe JXA-8200 with four wavelength-dispersive spectrometers. Operating conditions were 15 kV accelerating voltage, 15 nA specimen current, 20 s counting time (20 s peak, 10 × 2 s background) and 5 μm beam size.

4.6. Piezometry

Several empirical and theoretical piezometers have been calibrated, which relate differential stress and the size of dynamically recrystallized quartz grains formed during steady-state dislocation creep (Table 1). The difference between the piezometers lies in the value of the parameters b and r in an equation of the form:

$$\sigma = \left(\frac{D}{b}\right)^{1/r}, \tag{5}$$

where σ is the differential stress, D the diameter of quartz grains and b and r experimentally determined constants (Table 1).

In order to apply them to the deformation D3 in the principal dyke, quartz grains were traced on photomicrographs. Their area was measured making use of picture analysis software. The grain diameter is then calculated as the diameter of a circular particle of equal area.

5. Results

5.1. Deformation phases and microfabrics

The present work deals principally with the deformation phases referred to as D3 and D4. Nevertheless, a short overview about older deformation phases identifiable by optical microscopy is provided with the aim of documenting some aspects of the retrograde evolution of the rocks in our study area.

5.1.1. D1, only present in diatexite

This is the oldest deformation phase recognizable in the diatexites direct south of the Bayerischer Pfahl shear zone in the area between Saunstein and Freyung (see Fig. 1). It is recorded by very high temperature microfabrics (Fig. 5a). Amoeboid contacts between quartz and feldspar are the result of diffusion creep indicating high-grade conditions (Gower and Simpson, 1992). Quartz grains show subgrains with boundaries parallel

Table 1
Basic parameters for piezometers

	b	r
Twiss (1977, 1980)[a]	14,500	−1.47
Mercier et al. (1977)[a]	4,070	−1.4
White (1979)[a]	12,900	−1.43
Etheridge and Wilkie (1981)[a]	14,200	−1.47
Koch (1983)[a]	490	−0.59
Christie et al. (1980), wet[b]	1,780	−0.9
Stipp and Tullis (2003)	3,631	−1.26

[a] Taken from Abalos et al. (1996).
[b] Taken from Ord and Christie (1984).

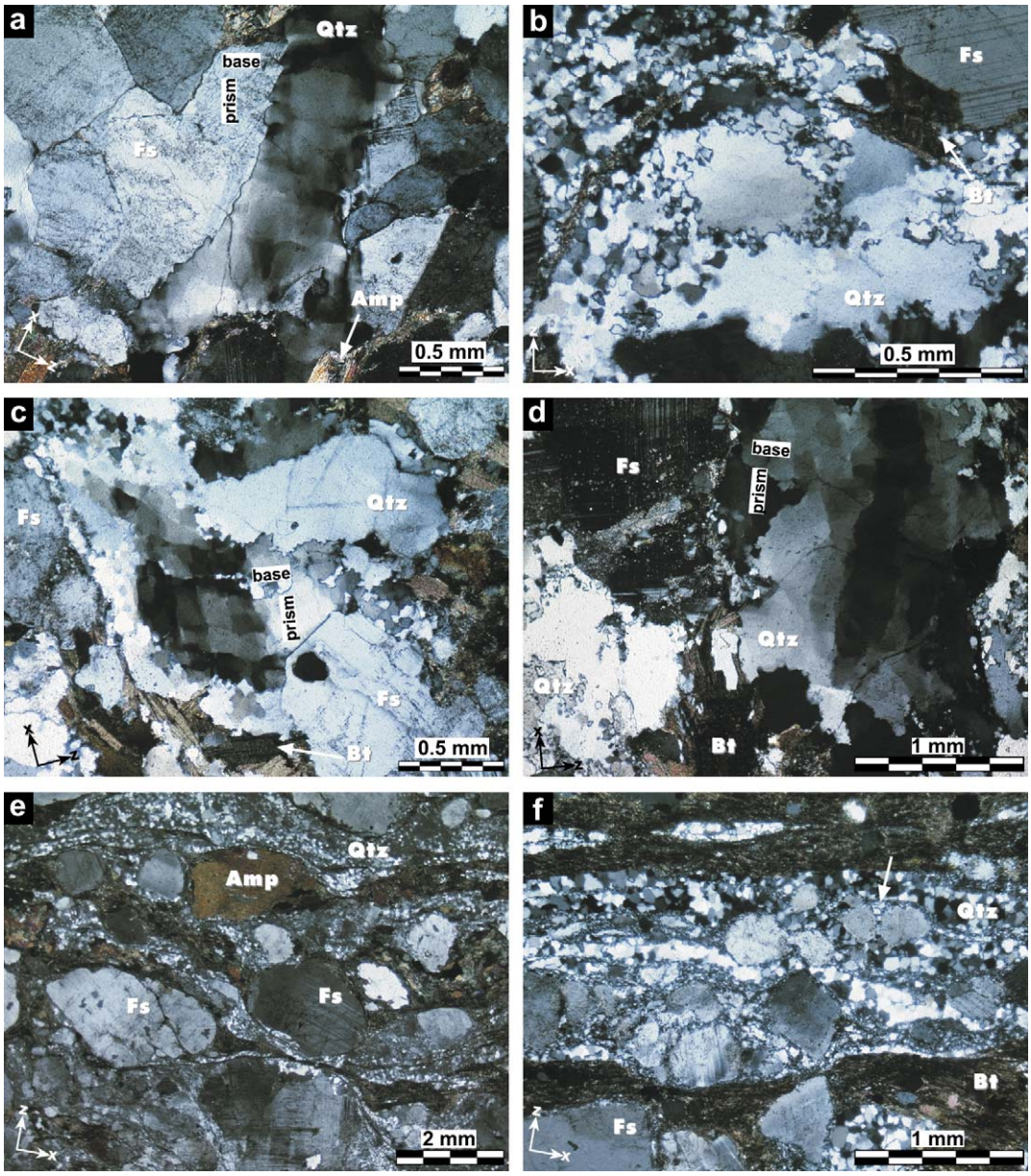

Fig. 5. Photomicrographs of diatexites affected by different deformation phases, *XZ* sections, crossed polarizers. (a) D1 in sample 141. This sample was collected 6 km west-southwest of the town Freyung (see Fig. 1), coordinates N 48°47′39.2″ E 013°28′34.9″. D1 is recorded by amoeboid contacts between quartz and feldspar and chessboard patterns in quartz. (b) D2 in sample 599. Mosaic-like pattern in quartz. (c) and (d) D2 in sample 92 (see also Fig. 6b). Chessboard pattern in relictic quartz old grains surrounded by recrystallized quartz. (e) and (f) D3 in sample 598. Quartz is completely recrystallized and feldspar is partly recrystallized. See text for further explanation. This figure can be viewed in color in the online version of this article.

to both prism and basal planes, defining a so-called chessboard pattern. The latter is thought to be diagnostic for prism <*c*> slip, which is active at temperatures higher than 600 °C in the β-quartz stability field (Mainprice et al., 1986; Masberg et al., 1992; Kruhl, 1996). This deformation phase produced a weak foliation defined by the shape-preferred orientation of minerals (mainly quartz, feldspar and biotite). D1 is found as a relict in areas with no or a very weak D2 overprint. The D1 kinematics is unknown.

5.1.2. D2, only present in diatexite

D2 is characterized by a variously, usually poorly developed, NW–SE trending tectonic foliation resulting from dextral simple shear (Fig. 6b). Photomicrographs of diatexites affected by D2 are presented in Fig. 5b–d. Quartz forms aggregates of new grains, in which relict old grains are abundant. New grains appear to be nearly strain free, whereas old grains present chessboard patterns. The chessboard pattern might be to some extent inherited from D1, since subgrain boundaries may be very stable microstructures in quartz (Kruhl, 1996), but this possibility is difficult to evaluate. Grain boundaries are strongly lobate or serrated due to grain boundary migration recrystallization, often with crystallographically controlled squared contours that constitute the so-called reticular or mosaic-like pattern (Gapais and Barbarin, 1986). Feldspar is incipiently recrystallized at grain borders and cracks. Although

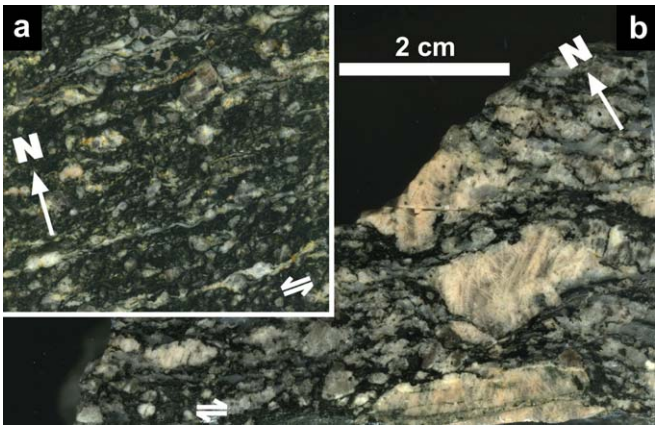

Fig. 6. Hand specimens of dark-colored diatexite, *XZ* sections, same scale for both specimens. (a) Sample 598 belongs to the Saunstein quarry (see Fig. 2 for location) and is affected by D3. (b) Sample 92 was collected 3 km west of the town Freyung (see Fig. 1, coordinates N 48°48′25.1″ E 013°30′22.5″) and is affected by D2. This figure can be viewed in color in the online version of this article.

temperature seems to have been high enough, the amount of strain was probably not sufficient to produce pervasive feldspar recrystallization, as proposed by Tullis and Yund (1977). Feldspar shows also patchy undulose extinction and microcracks and is in a few cases boudinaged or broken. Plagioclase is mechanically twinned and sometimes zoned. Lobate grain boundaries between feldspar and quartz are rare. Most of the mobile contacts between different phases were probably formed during D1 and destroyed during D2, since they represent a rather unstable microfabric element (Gower and Simpson, 1992). Amphibole often contains a diopsidic core and displays patchy undulatory extinction and subgrains. Biotite plates define the tectonic foliation. Biotite grains are always accompanied by a large number of tiny ($\sim$10 μm) titanite and/or ilmenite crystals at the borders or at exfoliation planes, suggesting crystallization of Ti-rich biotite at high temperature and Ti exsolution during temperature decrease. Dextral shear sense is deduced from σ-type mantled porphyroclasts.

5.1.3. D3 in diatexite

D3 is characterized by a well-developed, E–W trending mylonitic foliation resulting from sinistral simple shear. Apart from the orientation of the foliation, the sinistral sense of shear of this phase, as clearly indicated by σ-type mantled porphyroclasts, also differs from the kinematics of D2. It is important to note that dextral displacement along NW–SE trending planes (D2) and sinistral displacement along E–W trending planes (D3) cannot result from one single deformation phase. Therefore we consider sinistral shearing as a result of a post-D2 event, which will be referred to as D3.

D3 is accompanied by a considerable grain size reduction (Fig. 6a). Quartz forms lenticular aggregates and ribbons of equant new grains of strain-free appearance (Fig. 5e and f). Grain boundaries are mostly regular and straight, but some show also light serrated or sutured borders. A well-developed lattice preferred orientation is present, but no shape-preferred orientation. Chessboard patterns are lacking. Attending to these microfabric features, a combination of subgrain rotation and grain boundary migration are proposed as active recrystallization mechanisms. Feldspars are partially recrystallized forming core-and-mantle structures, σ-type mantled porphyroclasts and fine-grained polycrystalline ribbons. Local brittle behavior is also reported by some broken crystals. There is no evidence of diffusion creep at quartz/feldspar boundaries. Amphibole can be found as porphyroclast, often with a diopsidic core, and also forming part of the foliation planes together with biotite. New, small biotite grains grow in strain shadows and parallel to the foliation. The amount of titanite and ilmenite accompanying biotite is even higher than described for D2.

5.1.4. D3 in granite

D3 converts the granite in proto-, meso- or ultramylonite, depending on the considered location. These rocks can be described as type I *S–C* mylonites after Lister and Snoke (1984; see also Berthé et al., 1979). The increase in strain intensity towards the contact to the host rock is reflected by the reduction in grain size and the decreasing angle between *C* and *S* surfaces (Fig. 3). Looking at the different samples in detail, we can realize that the decrease of deformation intensity does not take place in a strictly progressive fashion, but rather changes back and forth on a meter scale with a generally decreasing trend on the outcrop scale. The most fine-grained specimens are found in two bands, one of them between 0 and 2 cm away from the contact to the host rock and the second one between 0.5 and 2 m away from the contact (schematically represented in Fig. 2).

Under the microscope (Fig. 7a and c) the most fine-grained samples are constituted by a very fine-grained quartz-feldspar matrix in which some cleavage domains of newly formed phengite are recognizable. Quartz and feldspar grains are completely mixed, with the exception of some rare bands of pure quartz. Some porphyroclasts of feldspar and igneous phengite are present. The configuration of asymmetric folds is compatible with a sinistral sense of shear (Fig. 3b).

In moderately to weakly strained areas (Fig. 7b, d, e, f and g) a fine banding of quartz and feldspar layers becomes visible, whereas phengite is more homogeneously distributed and does not form separate domains. Quartz and feldspar domains are easily identified due to the difference in grain size. Quartz occurs in the form of equigranular polycrystalline ribbons. Grain boundaries are straight and regular as well as irregular and lightly serrated. A lattice preferred orientation is present. Most of the grains appear to be strain-free; a few of them have prism-parallel subgrains or deformation bands. The quartz microfabrics present no differences compared to those described for D3 in the host rock. Grain boundary migration and subgrain rotation seem to have been likewise the dominant recrystallization mechanisms. Feldspar is partially recrystallized, forming fine-grained layers and σ-type mantled porphyroclasts, rarely δ-type ones. K-feldspar was replaced by albite at the margins (Fig. 8, Table 2), which points to a fluid-assisted deformation. Some porphyroclasts are transected by synthetic

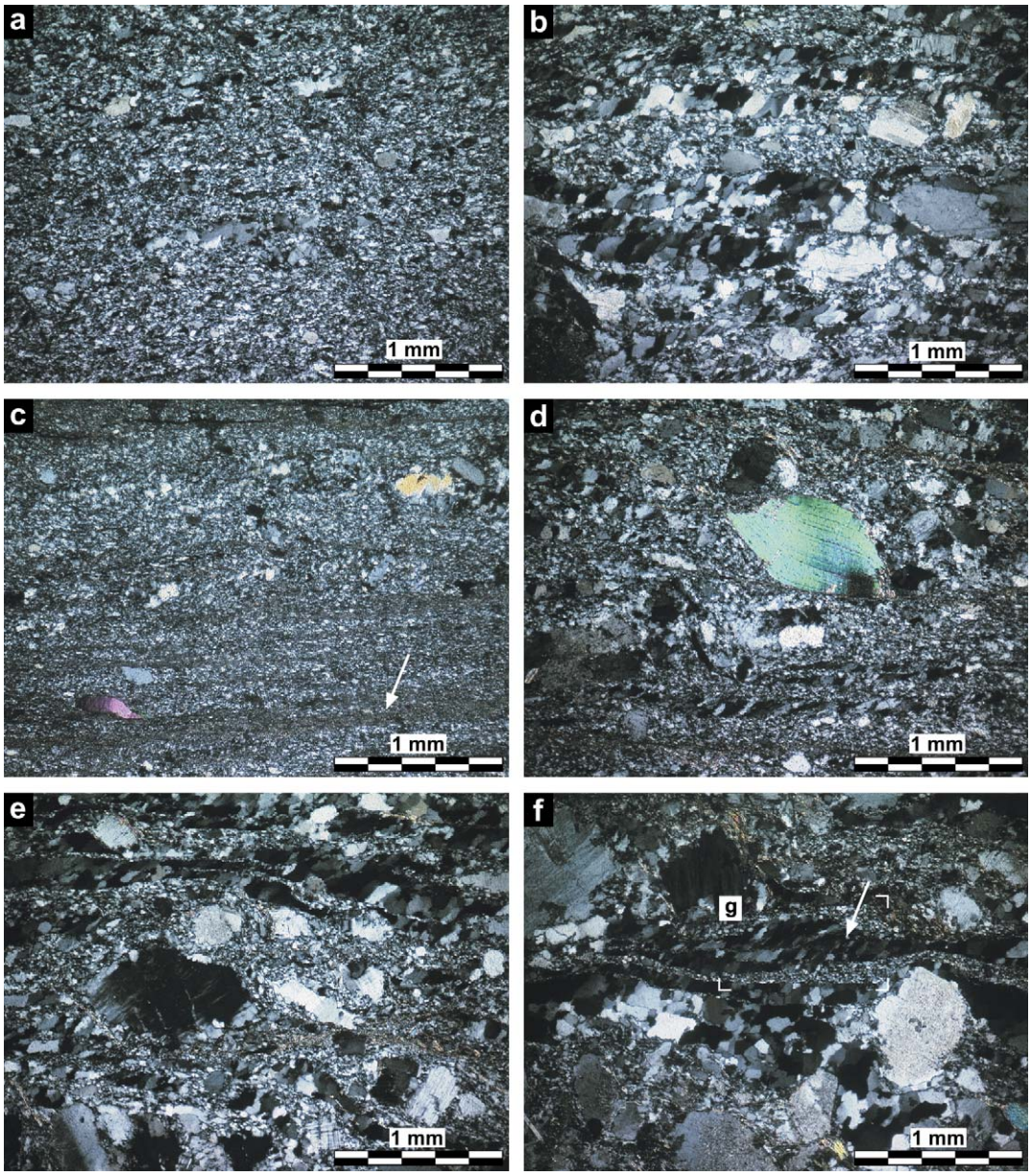

Fig. 7. Photomicrographs of granite samples affected by D3 and D4 in order of increasing distance to the host rock, *XZ* sections, crossed polarizers. (a) Sample 602. (b) Sample 603. D4 quartz shape-preferred orientation indicates dextral sense of shear. (c) Sample 606. The arrow indicates a cleavage domain constituted by newly formed phengite. (d) Sample 605. Mica-fish and angular relationship between *S* and *C* surfaces point to a sinistral sense of shear (D3), whereas the quartz shape-preferred orientation results from dextral simple shear (D4). The fine-grained matrix consists of recrystallized feldspar. (e) Sample 607. White mica and feldspar porphyroclasts are embedded in a matrix of alternating fine-grained feldspar layers and polycrystalline quartz ribbons. Note the sinistral sigmoidal fabric (D3) and dextral quartz shape-preferred orientation (D4). (f) Sample 608. The arrow indicates a band along which D4 concentrates, resulting in dextral quartz shape-preferred orientation. Below this band there are some other quartz layers which are practically not affected by D4 and show no shape-preferred orientation. (g) Enlargement of the former picture showing a quartz aggregate affected by D4. Grain boundaries are intensively sutured and fuzzy. (h) Sample 611. Quartz ribbons are slightly affected by D4, more intensively at the bottom right corner of the photograph. (i) Sample 615. Nearly undeformed granite. This figure can be viewed in color in the online version of this article.

or antithetic microfaults. Primary igneous feldspars were partially converted to phengite during grain-size reduction. Fine-grained phengite and biotite grow principally in strain shadows or at foliation surfaces. Igneous white mica typically forms mica-fishes and shows kinking. Igneous biotite is found as inclusions in feldspar or dispersed in the matrix. Sinistral shear sense is reported by σ-type mantled porphyroclasts, mica fishes, monomineralic sigmoidal bands and the angular relationship between *S* and *C* surfaces.

Considering all microfabric aspects of D3, some constraints on the deformation temperature can be made: (i) the transition from dominant subgrain rotation recrystallization to dominant grain boundary migration recrystallization is proposed by Stipp et al. (2002) to be approximately between 480 and 530 °C ($P \sim 2.5-3$ kbar); (ii) after Kruhl (1996) the absence of chessboard patterns in quartz does not allow any major constraint in our case, since the pressure during deformation is unknown, but even assuming middle crust pressures, the

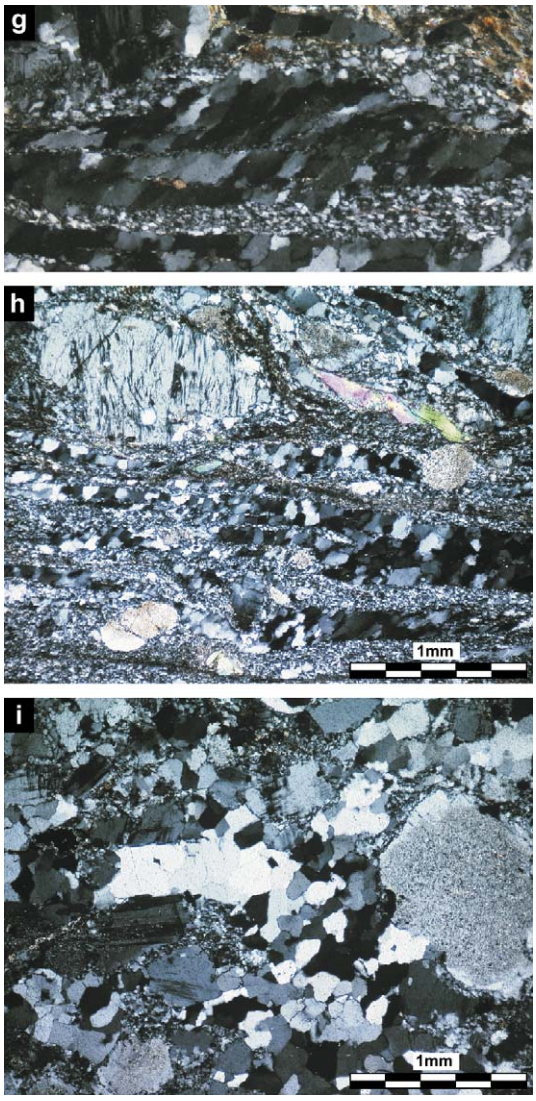

Fig. 7 (*continued*)

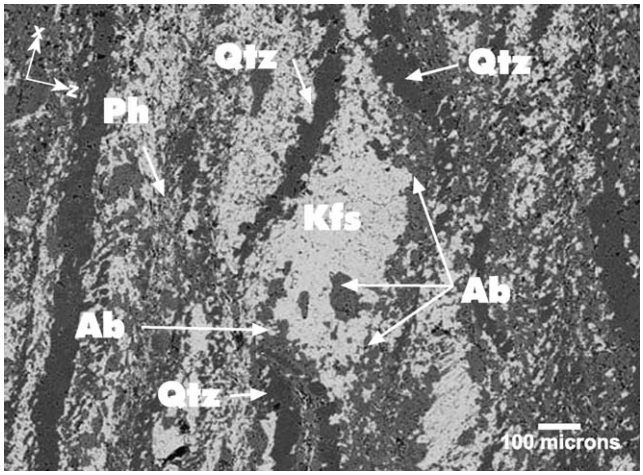

Fig. 8. Backscattered electrons image showing the chemical variations between feldspar core and mantle in sample 605. Minerals in order of increasing brightness: quartz (Qtz), albite (Ab), K-feldspar (Kfs) and phengite (Ph).

Table 2
Electron microprobe analyses of feldspars from sample 605

		Ca^{2+}	Na^{+}	K^{+}	Si^{4+}	Al^{3+}	Total
Porphyroclast 1	Mantle	0.11	0.84	0.01	2.93	1.07	4.96
		0.11	0.84	0.01	2.90	1.10	4.97
		0.12	0.84	0.01	2.90	1.10	4.97
		0.06	0.88	0.01	2.97	1.04	4.95
	Core	0.00	0.04	1.01	3.01	0.97	5.03
		0.00	0.04	0.97	3.01	0.98	5.01
		0.00	0.05	0.96	3.00	0.99	5.01
		0.00	0.10	0.92	3.00	0.99	5.02
		0.00	0.09	0.93	3.00	0.99	5.01
Porphyroclast 2	Mantle	0.08	0.88	0.01	2.95	1.05	4.97
		0.12	0.84	0.01	2.92	1.08	4.97
		0.09	0.90	0.01	2.94	1.06	4.99
	Core	0.00	0.03	1.00	3.01	0.98	5.02
		0.00	0.05	0.97	3.01	0.98	5.01
		0.00	0.03	1.00	3.01	0.98	5.02
		0.00	0.03	0.99	3.01	0.98	5.01
		0.00	0.03	0.99	3.01	0.98	5.02
		0.00	0.03	0.98	3.01	0.98	5.01
Porphyroclast 3	Core	0.00	0.06	0.97	3.01	0.98	5.02
		0.00	0.06	0.97	3.01	0.98	5.02
		0.00	0.04	0.99	3.00	0.99	5.03
		0.00	0.04	0.99	3.00	0.99	5.02
		0.00	0.04	1.00	2.99	0.99	5.03
	Mantle	0.08	0.87	0.01	2.95	1.06	4.96
		0.10	0.86	0.01	2.91	1.09	4.98
Porphyroclast 4	Mantle	0.07	0.89	0.01	2.94	1.07	4.98
		0.07	0.80	0.00	3.06	0.93	4.88
		0.10	0.86	0.01	2.92	1.09	4.98
		0.07	0.89	0.01	2.94	1.06	4.98
	Core	0.00	0.04	0.99	3.00	0.99	5.02
		0.00	0.04	0.97	3.00	0.99	5.01
		0.00	0.03	1.00	3.00	0.99	5.02
		0.00	0.04	0.98	3.00	0.99	5.02
		0.00	0.04	0.99	3.00	0.99	5.02
Porphyroclast 5	Core	0.00	0.04	0.99	3.00	0.99	5.02
		0.00	0.07	0.96	3.00	1.00	5.02
		0.00	0.05	0.98	3.00	0.99	5.02
		0.00	0.07	0.95	3.00	0.99	5.01
		0.00	0.04	0.98	3.00	0.99	5.01
	Mantle	0.03	0.92	0.01	2.98	1.03	4.97

Cations calculated by charge balance assuming 8 oxygen atoms per formula unit. Ba and Fe were also analyzed: their concentration as oxides is always below 0.1 wt% and is not listed. K-rich porphyroclasts developed a Na-rich mantle during deformation (see also Fig. 8). The average composition of feldspars is An_0 Ab_5 Or_{95} at cores and An_9 Ab_{90} Or_1 at mantles.

maximum deformation temperature is above or around the wet granite solidus, which represents in fact no constraint at all; (iii) the lack of mobile boundaries between different phases indicates that diffusion creep did not play an important role in deformation; thus, the deformation must have taken place well under solidus conditions; (iv) feldspar deforms by dislocation creep at temperatures above 450–500 °C, the presence of fluids can have contradictory effects (microcracking and recrystallization favored by a chemical free energy term; Tullis, 1983), which are difficult to evaluate in terms of deformation temperature. In summary, assuming a deformation temperature around 500–550 °C seems to be reasonable.

5.1.5. D4, in granite

While σ-type porphyroclast systems and other monoclinic fabric elements (e.g. mica fishes, sigmoidal bands and ribbons) indicate clearly a sinistral sense of shear during D3 in the granite dyke, the oblique foliation defined by the shape-preferred orientation in many quartz aggregates displays a dextral shear sense (Fig. 7b, d, e, f and g). This phenomenon could be explained in three ways:

(i) The quartz shape-preferred orientation is older than the whole D3 fabric. A pre-D3 dextral event produced the quartz shape-preferred orientation, which remains preserved as a relict.
(ii) The quartz shape-preferred orientation and the D3 fabric formed together, i.e., there is some unknown mechanism producing ''anomalous'' shape-preferred orientation of quartz grains under certain conditions.
(iii) The quartz shape-preferred orientation is younger than the whole D3 fabric. A new deformation phase (D4) of very low intensity overprinted not the whole fabric, but only the shape-preferred orientation of quartz.

The first possibility is improbable: D3 produced a very strong monoclinic symmetry and a considerable amount of strain; feldspar recrystallized and formed well-developed σ-type mantled porphyroclasts and fine-grained bands; in sum, the strain amount and the temperature were too high for the preservation of old structures in quartz during D3 and resetting of its fabric is to be expected.

The second hypothesis lacks experimental support. Such a phenomenon has not been described up to now. Moreover, the fact that many but not all quartz ribbons present this ''anomalous'' shape-preferred orientation (Fig. 7f) does not support a common development of shape-preferred orientation and D3 fabric, but rather a separate formation of the D3 fabric and the quartz shape-preferred orientation.

Thus, the third option seems the most probable. As a microstructural evidence for the quartz shape-preferred orientation being post-D3, we observed that even in polycrystalline quartz ribbons, whose sigmoidal form displays clearly a sinistral shear sense, the shape-preferred orientation shows a dextral sear sense (Fig. 7d and e): the opposite temporal succession would have destroyed the dextral shape-preferred orientation of quartz. Quartz grain boundaries are not squared and sharp as observed in D3 (Fig. 7), but intensively sutured and fuzzy (Fig. 7g) indicating grain boundary migration recrystallization and a deformation temperature slightly lower to that during D3. The percentage of quartz aggregates displaying dextral shape-preferred orientation increases towards the contact to the host rock, suggesting that during D4 this contact continued to play an important role.

5.2. Quartz textures obtained by means of electron backscatter diffraction

Six granite samples located at different distances to the contact, and therefore variously deformed, were selected and scanned on *XZ* sections. The obtained *a* and *c* axes patterns are represented in Fig. 9. In the diagrams shown a clustering of quartz *c* axes parallel to the intermediate *Y* axis of the finite strain ellipsoid is obvious. *a* axes patterns develop two secondary maxima on the *XZ* plane and one principal maximum on the *XZ* plane parallel to C. The latter is deviated with respect to the *X* axis of the finite strain ellipsoid indicating sinistral sense of shear (Simpson and Schmid, 1983; Schmid and Casey, 1986). This lattice preferred orientation pattern is diagnostic for prism $<a>$ slip in quartz, which is known to be dominant at middle to high temperature conditions, that is, at upper greenschist to amphibolite facies conditions (Bouchez and Pêcher, 1981; Schmid and Casey, 1986; Jessell and Lister, 1990; Law, 1990). After Stipp et al. (2002) this pattern is diagnostic for the transition between grain boundary migration recrystallization and subgrain rotation recrystallization, which corroborates the results of our microfabric analyses (see above) and is in good agreement with a deformation temperature of 500–550 °C.

It is not possible to infer a shear sense from the *a* axes pattern of sample 603, in which *S* and *C* surfaces are parallel. In the most fine-grained sample (sample 606, Figs. 3b and 9) the fabric is more poorly developed than in the other samples. This phenomenon has already been observed by other authors (Berthé et al., 1979) and could be a result of operating deformation mechanisms that do not promote or even prevent the development of lattice preferred orientation, such as grain boundary sliding with more or less contribution of diffusion creep, since grains slide past each other more easily in fine-grained aggregates than in coarser-grained ones (Behrmann, 1985; Behrmann and Mainprice, 1987; Boullier and Gueguen, 1975). Sample 615 is macroscopically nearly undeformed but shows some weak crystallographic fabric. Maxima are in this case displaced with respect to the principal strain axes due to the uncertainty about their position during sample preparation, since foliation and lineation are lacking.

The effect of D4 on the lattice preferred orientation patterns is impossible to quantify. In relation to this deformation phase, we should emphasize that both temperature and shear sense inferred from lattice preferred orientation patterns are compatible with D3 and therefore (i) D4 must have been very weak and/or (ii) the averaging effect of the method results in patterns showing predominantly D3.

Quartz in diatexites shows a much weaker lattice preferred orientation, probably due to the lower quartz content, which leads to a stronger interaction between quartz and other minerals and prevents quartz grains from recrystallizing without obstacles. Whereas the lattice preferred orientation patterns of sample 92, which is representative for D2, are hardly interpretable, the ones of sample 598, representative for D3, are fairly well developed and show a similar appearance as in the granite dyke. Thus, it is corroborated that the deformation D3 observed in granite and host rock took place under similar temperature conditions.

5.3. Finite strain of the principal dyke

The results obtained from the strain analysis using the R_f/Φ' method are represented in Table 3 and Fig. 10. It is important to note that R_s is an underestimation of the real strain, since

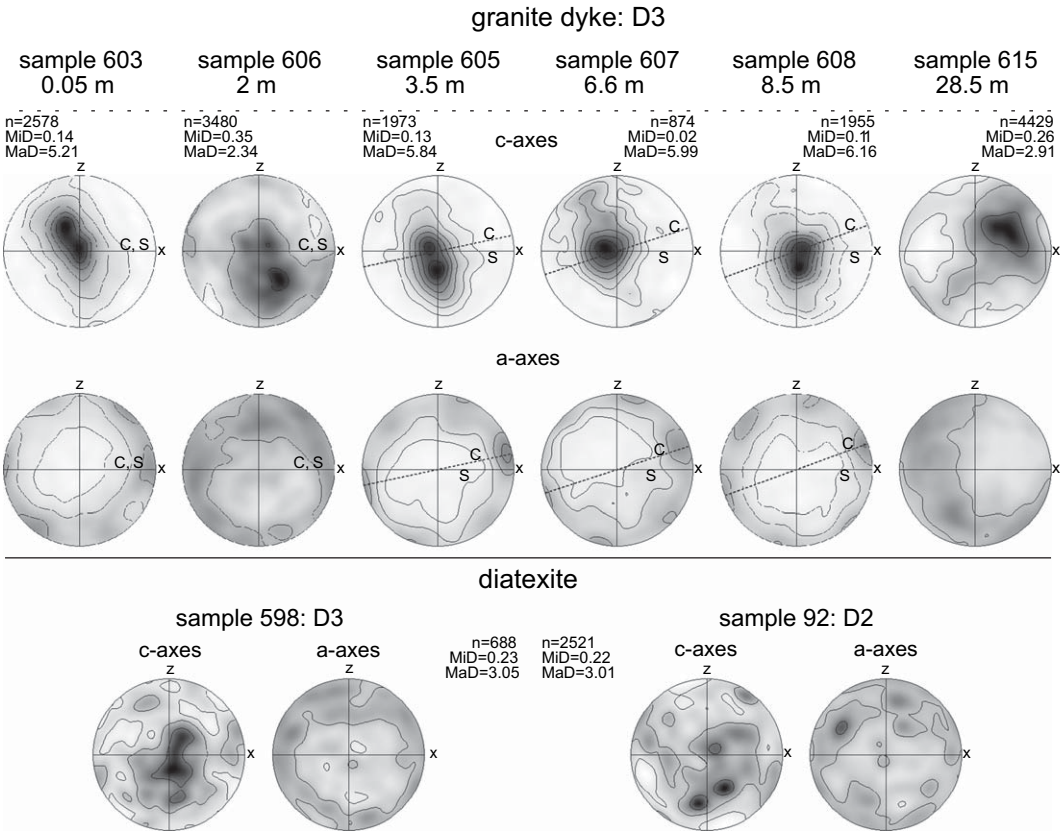

Fig. 9. Stereographic representation of quartz *c* and *a* axes obtained by means of electron backscatter diffraction. Equal area projection, lower hemispheres. *n*, number of data points; MiD, minimum density; MaD, maximum density. Contours at 0.5, 1, 2, 3, 4, 5, 6, 7. Black represents the maximum intensity. Data points were smoothed with a Gaussian of 10° full width half maximum.

feldspars exist in the deformed granite not only as porphyroclast, but also as completely recrystallized, fine-grained aggregates in the matrix, which could not be taken into account in our measurements due to their small thickness at hand specimen scale. Moreover, feldspar crystals contribute to the bulk strain not only by ductile behavior but also by rotation. Finally, the strain measured in feldspar porphyroclasts is surely lower than the bulk strain, since the matrix contains a large amount of quartz, which was likely weaker and is expected to have suffered a higher strain than the porphyroclasts.

Two aspects of our results are notable:

- The magnitude of strain increases towards the contact to the host rock (Fig. 10a, b).
- The form of the finite strain ellipsoid in different points of the dyke was plotted in a Flinn graph (Fig. 10c): oblate ellipsoids ($S > L$) are obtained, with the flattening being most pronounced near the contact. This result is visually corroborated by the fact that the planar fabric of the deformed granite dyke is best developed next to the contact to the host rock.

In Table 3 the strain calculated from the angle between *S* and *C* planes is shown. As obtained from the R_f/Φ' method, the finite strain ellipsoid plots on the flattening field and therefore the plane-strain requirement for the strain calculation from the angle between *S* and *C* planes is not fulfilled. Therefore, the reported γ values might contain some error.

Table 3
Finite strain data calculated by the R_f/Φ' method using the computer program "STRAIN" (Unzog, 1990) and by the angle between *S* and *C* planes

Sample	Distance to contact (m)	After Peach and Lisle (1979)				After Ramsay and Huber (1983)				After Ramsay and Graham (1970)	
		R_s			k	R_s			k	θ'	γ
		$R_{s,xz}$	$R_{s,yz}$	$R_{s,xy}$		$R_{s,xz}$	$R_{s,yz}$	$R_{s,xy}$			
606	2.0	2.94	2.24	1.31	0.25	3.37	2.57	1.31	0.20	–	–
605	3.5	2.59	1.79	1.45	0.45	2.66	1.86	1.43	0.50	12°	4.5
607	6.6	2.33	1.76	1.32	0.43	2.58	1.85	1.39	0.46	18°	2.7
608	8.5	1.99	1.61	1.24	0.39	2.16	1.72	1.26	0.36	20°	2.4

R_s, ellipticity of the strain ellipse.

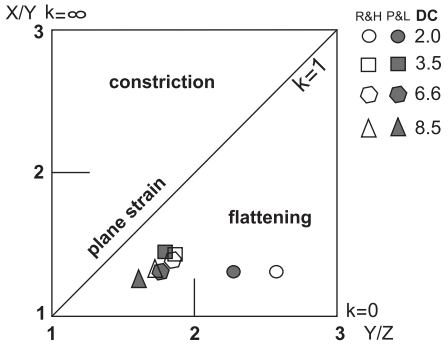

Fig. 10. Flinn graph showing the finite strain geometry calculated by the R_f/Φ' method at different locations of the principal dyke. White and gray symbols represent the strain calculated after Ramsay and Huber (1983) and Peach and Lisle (1979), respectively. DC, distance to the contact (m).

5.4. Mass transfer, volumetric strain and Zr thermometry

There is some evidence of the presence of a fluid phase during D3. Electron microprobe analyses (Table 2) show a change in feldspar composition: K-feldspar (An_0 Ab_5 Or_{95}) is substituted by plagioclase (An_9 Ab_{90} Or_1) during dynamic recrystallization (Fig. 8). The second evidence is constituted by the fine-grained phengite growing parallel to the mylonitic foliation, whose formation, probably at the expense of igneous feldspar, needs the presence of a fluid phase.

The isocon-diagram method (Grant, 1986) was applied in order to evaluate the effect of the fluids present during D3. The results in Table 4 and Fig. 11 show most of the mobile and immobile components plotting next to or on a line of slope = 1. We can therefore conclude that deformation did not lead to an important mass exchange between the sheared granite and the surrounding rocks, despite a fluid being present and enhancing the mobility of some components. No significant volume change took place during deformation. Nevertheless, some K and Ba loss is observed, maybe due to the transformation of K-feldspar into phengite. The higher Ca content in strained areas is coupled with the aforementioned transformation of K-feldspar into plagioclase during deformation. The required additional Ca might have been supplied by the host rock.

From the zirconium content of the samples a temperature of 716 ± 18 °C was calculated. After Siebel et al. (2005), the granitic dyke is peraluminous; zircons display magmatic zoning and show no clear evidence for the presence of inherited cores. Therefore, the conditions for the application of the zircon solution model by Watson and Harrison (1983) are fulfilled. However, it is important to remark that this Zr thermometer is based upon experiments above 860 °C, so that the obtained temperature might be relatively imprecise.

5.5. Differential stress

We calculated the differential stress using piezometers from several authors (Table 5, Fig. 12). Although D4 had an important effect on quartz oblique orientation, this deformation affected quartz grain size and shape significantly only in some identifiable discrete bands. These overprinted bands were excluded from our analysis and only quartz grains included in monomineralic bands without shape-preferred orientation were used. In these monomineralic bands the size of quartz grains remains nearly constant and steady-state dislocation creep was presumably reached during dynamic recrystallization. The obtained differential stress should therefore approximate the stress governing D3. All piezometers show similar tendencies, with the differential stresses increasing towards

Table 4
XRF analyses of different granite samples in order of increasing distance to the host rock

Sample	Distance to contact (m)	LOI (%)	Total	SiO_2	Al_2O_3	Fe_2O_3	MnO	MgO	CaO	Na_2O	K_2O	TiO_2	P_2O_5
603	0.05	0.23	99.93	76.12	13.15	0.93	0.023	0.16	0.75	3.86	4.54	0.06	0.02
604	0.5	0.33	99.89	76.79	13.00	0.74	0.033	0.12	0.63	3.50	4.61	0.06	0.02
605	3.5	0.47	100.02	76.97	13.40	0.89	0.044	0.12	0.66	3.28	4.03	0.07	0.02
608	8.5	0.83	100.78	76.47	12.94	1.06	0.041	0.18	1.00	3.15	4.96	0.07	0.02
610	11	0.43	100.47	76.78	12.95	0.97	0.037	0.14	0.35	3.28	5.38	0.06	0.02
615	28.5	0.37	100.80	76.42	13.23	0.86	0.025	0.17	0.42	3.42	5.70	0.07	0.03
		Ce	Cr	Ga	La	Nb	Nd	Ni	Pb	U	V	Zr	
603	0.05	55	18	16	21	51	16	41	23	11	6	44	
604	0.5	75	4	16	10	46	27	18	30	14	3	50	
605	3.5	80	2	14	27	29	28	12	33	11	5	68	
608	8.5	67	10	16	20	29	27	23	32	15	2	69	
610	11	71	13	15	23	28	17	12	28	4	5	68	
615	28.5	66	5	15	15	31	14	19	25	5	5	72	
		As	Ba	Co	Cs	Cu	Rb	Sn	Sr	Th	Y	Zn	
603	0.05	5	192	37	15	6	326	9	107	30	78	1	
604	0.5	6	26	55	21	2	462	11	28	26	108	5	
605	3.5	6	27	83	20	6	455	14	32	34	115	10	
608	8.5	6	39	66	12	2	430	14	41	37	116	9	
610	11	6	34	95	14	1	498	13	31	35	107	4	
615	28.5	6	206	91	13	2	392	6	92	42	85	<LLD	

These data were used in the application of the isocon-diagram method (Fig. 11) and the Zr thermometry.

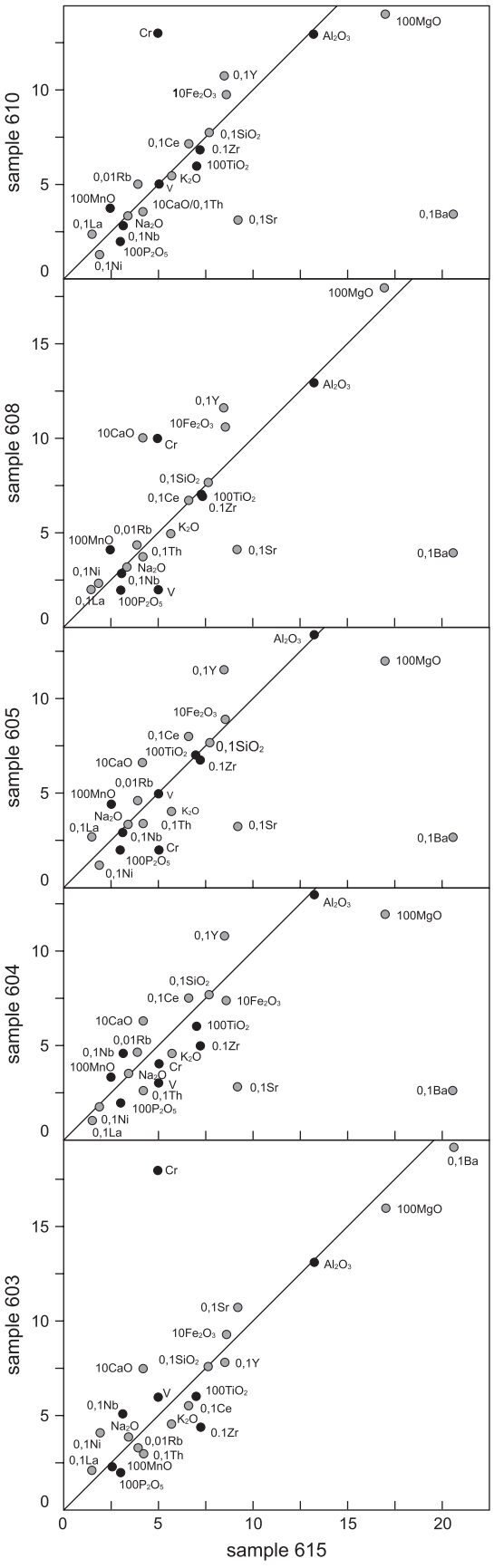

Fig. 11. Isocon diagrams plotting deformed sample vs. undeformed sample in order of increasing deformation intensity (see Fig. 2 for location). In all diagrams the *X* axis represents the concentration in sample 615 (undeformed). Oxides in weight percent, elements in ppm. Gray and black points represent mobile and immobile components, respectively.

the contact to the host rock, that is, towards more strained areas. Differential stresses range between ~10 und 60 MPa in the analyzed specimens.

6. Discussion

6.1. Deformation history

The observed microstructures reflect the retrograde evolution of the rocks, cooling down from high-temperature conditions during D1 down to amphibolite to greenschist facies during D2, D3 and D4. Structures formed by dislocation creep overprinted older ones originated by diffusion creep. The dextral displacement along NW–SE trending planes during D2 is not compatible with the sinistral movement along E–W trending planes during D3. Thus, a change of the stress state governing D2 is necessary to explain D3. D4 could represent the return to a stress state similar to the one present during D2. From the microfabric analysis we must conclude that the dyke did not intrude synkinematically, since the deformation temperature should have been around 500–550 °C and dyke and host rock were thermically equilibrated during deformation. The host rock was at the time of intrusion well under the temperature of granitic solidus, as can be inferred from the existence of chilled margins.

6.2. Strain gradient, strain geometry and geochemical data

Strain increases towards the contact to the host rock. No significant volume change took place during deformation. The strain geometry presented in Section 5.5 is therefore a real geometry and not the result of volumetric strain: the dyke constitutes a closed chemical system at the outcrop scale, in which the mineral transformations visible at the microscope scale remained nearly isochemical. Flattening strain suggests transpression during the main phase of shearing (e.g. Sanderson and Marchini, 1984; Tikoff and Fossen, 1999).

6.3. Stress data, strain localization and rheology

D3 is observable most of all in the principal granite dyke and affects the host rock only to a lesser extent. The intensity of D3 is higher near the contact to the host rock. If (i) the intrusion was not synkinematic and therefore there was no melt present at the time of deformation and (ii) during the deformation the temperature was equilibrated inside the dyke and between the dyke and the host rock, why does the deformation concentrate in the dyke and preferentially at the contact to the host rock? The contact must have played an important

Table 5
Differential stresses calculated using the piezometers listed in Table 1

	Sample 606 ($D = 48 \pm 18$ μm, $N = 61$)		Sample 605 ($D = 86 \pm 25$ μm, $N = 60$)		Sample 607 ($D = 122 \pm 37$ μm, $N = 87$)		Sample 608 ($D = 130 \pm 42$ μm, $N = 84$)	
	σ (MPa)	Error	σ (MPa)	Error	σ (MPa)	Error	σ (MPa)	Error
Twiss (1977, 1980)[a]	49	+19, −10	33	+9, −5	26	+7, −4	25	+8, −4
Mercier et al. (1977)[a]	24	+10, −5	16	+4, −3	12	+4, −2	12	+4, −2
White (1979)[a]	50	+20, −10	33	+9, −5	26	+7, −4	25	+8, −4
Etheridge and Wilkie (1981)[a]	48	+19, −10	32	+9, −5	25	+7, −4	24	+8, −4
Koch (1983)[a]	52	+67, −22	19	+15, −7	11	+9, −4	10	+9, −4
Christie et al. (1980), wet[b]	56	+40, −17	29	+14, −7	20	+10, −5	18	+10, −5
Stipp and Tullis (2003)	31	+15, −7	20	+6, −4	15	+5, −3	14	+5, −3

D, particle diameter; *N*, number of particles measured.
[a] Taken from Abalos et al. (1996).
[b] Taken from Ord and Christie (1984).

role during D3. It probably represented a rheological boundary at which hard, feldspar-rich diatexite and soft, quartz-rich granite met. Stresses concentrate at the contact surface, affecting predominantly the softest rock type. In a first phase of D3, the concentration of stresses at the rheological boundary and their dissipation towards the centre of the dyke originated a stress distribution which might have been similar to that represented in Fig. 12. This stress distribution caused a strain and strain-rate gradient. As a consequence, the strain-rate gradient was probably responsible for a viscosity decay at the contact, promoting further strain localization and fluid access. The reduction in grain size promotes grain boundary sliding. The presence of a fluid gives way to reaction softening or hydrolytic weakening and formation of phengite in cleavage domains. Phengite contributed to the softening of the rock by accommodating strain by frictional sliding along (001) planes. The stresses measurable from quartz grain size probably represent mainly the stress governing the first phase, since the deformation in the second phase was dominated not by dynamic recrystallization but rather by frictional or grain boundary sliding in cleavage domains and fine-grained microlithons.

The fabric associated with D4 was only found in granite and is also stronger towards the contact; thus, this contact seems to have continued to control the strain distribution at the time of D4.

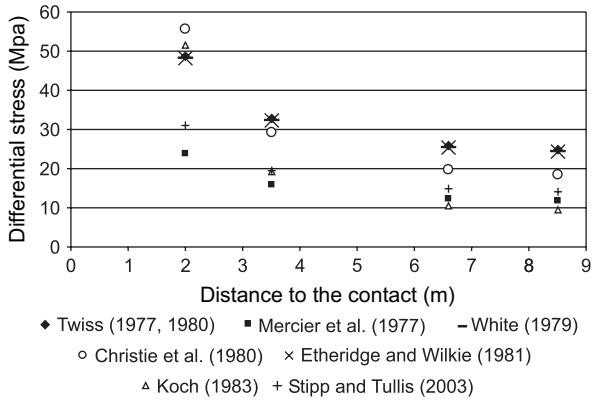

Fig. 12. Differential stress calculated from quartz piezometers calibrated by different authors. Error bars were omitted for simplicity. See errors in Tables 5 and 1 for further details.

6.4. Electron backscatter diffraction data

An evolution of *a* and *c* axes patterns depending on the distance to the host rock is not observed, with the exception of sample 606, and therefore a change in deformation temperature throughout the dyke must be ruled out. A homogeneous temperature inside the dyke implies automatically that temperature equilibrium was reached between host rock and dyke at the time of deformation. Intracrystalline slip in quartz took place predominantly along prism planes in the <*a*> direction. The recrystallization mechanisms were grain boundary migration and subgrain rotation. In the most strained bands (sample 606) the obtained texture seems to be the result of competing deformation mechanism, some of them favoring and others preventing the formation of a lattice preferred orientation, that is, dislocation creep was partially or fully substituted by grain boundary sliding ± diffusion creep in fine-grained areas. This change in deformation mechanisms could have contributed to the softening of the rock. Lattice preferred orientation patterns are compatible with D3 and therefore the influence of D4 on the lattice preferred orientation of quartz grains must have been very weak.

6.5. Reliability of shape-preferred orientation as shear-sense indicator

The oblique foliation defined by quartz shape-preferred orientation (D4) probably reflects a reactivation of the shear zone under dextral regime. In high strained parts of the granite dyke *S* and *C* surfaces became parallel to one another, sigmoidal structures are absent und porphyroclasts are scarce. The only available shear-sense indicators here are a few asymmetric folds and quartz shape-preferred orientation. By examining these high strained rocks one could interpret the deformation in the shear zone as having been produced by a single, dextral episode, which would have important consequences on the regional interpretation of the shear zone in relation to other major shear zones: a dextral, E–W trending shear zone can be interpreted as a subsidiary surface inside the Bayerischer Pfahl

shear zone system. Mattern (1995) also reported a quartz shape-preferred orientation in conflict with the other kinematic indicators at the Bayerischer Pfahl shear zone, but this time showing a bulk dextral sense of shear with a sinistral overprint inferred from the quartz shape fabric. The relationship between the deformation phases described by Mattern (1995) and in this paper cannot be established at present, but it seems clear that ''anomalous'' quartz oblique foliations are not a rare phenomenon in the Bavarian Forest. Abalos et al. (1996) have also reported shape fabrics in disagreement with other shear-sense indicators in rocks from Cabo Ortegal (Iberian Massif), which they interpret as caused by quartz annealing processes. We emphasize that caution is needed when inferring shear sense from quartz oblique foliation, since it can be overprinted with very low strains and consequently can only represent the very last deformation increment.

7. Conclusions

The main conclusions of our study are summarized as follows:

(i) The Saunstein granite dyke intruded under a stress field that interrupted for some time the stress field that caused D2 at the Bayerischer Pfahl shear zone and parallel or subsidiary surfaces. It intruded in a relatively cold host rock after the regional high-*T*/low-*P* metamorphism.

(ii) The dyke suffered sinistral shear after cooling down to ~500–550 °C during retrograde amphibolite to greenschist facies metamorphism and suffered a weak dextral reactivation under slightly lower temperature. During the deformation the contact to the host rock acted as a decoupling surface, which causes the deformation to concentrate in the softest rock type near the contact.

(iii) Dyke and host were thermically equilibrated during deformation. Thus, differences between the rheological behavior of diatexite and granite are not due to contrasting temperatures, but rather to contrasting mineralogy.

(iv) The deformation of the dyke is characterized by dramatic softening and strain localization at its margin due to several interacting processes: the initial strain localization started a series of feedback processes leading to further strain localization. Increasing strain caused grain size reduction and change of the main deformation mechanisms in quartz from intracrystalline glide accommodated by grain boundary migration recrystallization and subgrain rotation recrystallization to grain boundary sliding ± diffusion creep, which may have considerably reduced flow strength. The formation of phengite domains might have also contributed to the softening of the rock.

(v) The geometry of the finite strain ellipsoid is oblate. No significant volume change occurred during deformation, which implies that the flattening is a real strain geometry. This indicates that shearing took place under transpression.

(vi) Quartz oblique foliation represents a reliable shear-sense indicator only for the very last deformation increment. This can constitute on the one hand an advantage for detecting late inversions of shear sense, but can on the other hand be misleading when being used without corroboration from other indicators.

Acknowledgements

We gratefully acknowledge financial support by EU and Bavarian government and XRF analyses from the Bayerisches Landesamt für Umwelt. We wish to thank M.G. Bjornerud for a very constructive review.

References

Abalos, B., Azcarraga, J., Gil Ibarguchi, J.I., Mendia, M.S., Santos Zalduegui, J.F., 1996. Flow stress, strain rate and effective viscosity evaluation in a high-pressure metamorphic nappe (Cabo Ortegal, Spain). Journal of Metamorphic Geology 14, 227–248.

Artmann, C., 2001. Erläuterungen zur geologischen Karte 7146 Grafenau (NW-Teil, nördlich Schönberg) und Untersuchungen zu den felsmechanischen Kennwerten der Mylonite der Pfahlzone. Diploma thesis, Technische Universität München.

Beer, W.W., 1981. Die strukturelle Entwicklung der Metamorphite des Bayerischen Waldes. PhD thesis, Georg-August-Universität zu Göttingen.

Behrmann, J.H., 1985. Crystal plasticity and superplasticity in quartzite: a natural example. Tectonophysics 115, 101–129.

Behrmann, J.H., Mainprice, D., 1987. Deformation mechanisms in a high-temperature quartz-feldspar mylonite: evidence for superplastic flow in the lower continental crust. Tectonophysics 140, 297–305.

Behrmann, J.H., Tanner, D.C., 1997. Carboniferous tectonics of the Variscan basement collage in eastern Bavaria and western Bohemia. Geologische Rundschau 86 (Suppl.), 15–27.

Berthé, D., Choukroune, P., Jegouzo, P., 1979. Orthogneiss, mylonite and non coaxial deformation of granites: the example of the South Armorican Shear Zone. Journal of Structural Geology 1, 31–42.

Blaha, U., in press. Geologische Karte von Bayern 1:25 000, Erläuterungen zum Blatt Nr. 7145 Schöfweg. Bayerisches Geologisches Landesamt, München.

Bouchez, J.L., Lister, G.S., Nicolas, A., 1983. Fabric asymmetry and shear sense in movement zones. Geologische Rundschau 72, 401–419.

Bouchez, J.L., Pêcher, A., 1981. The Himalayan Main Central Thrust pile and its quartz-rich tectonites in central Nepal. Tectonophysics 78, 23–50.

Boullier, A.M., Gueguen, Y., 1975. SP-Mylonites: origin of some mylonites by superplastic flow. Contributions to Mineralogy and Petrology 50, 93–104.

Brandmayr, M., Dallmeyer, R.D., Handler, R., Wallbrecher, E., 1995. Conjugate shear zones in the Southern Bohemian Massif (Austria): implications for Variscan and Alpine tectonothermal activity. Tectonophysics 248, 97–116.

Büttner, S., Kruhl, J.H., 1997. The evolution of a late-Variscan high-T/low-P region: the southeastern margin of the Bohemian massif. Geologische Rundschau 86, 21–38.

Chen, F., Siebel, W., 2004. Zircon and titanite geochronology of the Fürstenstein granite massif, Bavarian Forest, SW Bohemian Massif: pulses of the late Variscan magmatic activity. European Journal of Mineralogy 16, 777–788.

Christie, J.M., Ord, A., Koch, P.S., 1980. Relationship between recrystallized grain size and flow stress in experimentally deformed quartzite. EOS Transactions American Geophysical Union 61, 377.

Christinas, P., Köhler, H., Müller-Sohnius, D., 1991. Alterstellung und Genese der Palite des Vorderen Bayerischen Waldes (Nordostbayern). Geologica Bavarica 96, 87–107.

Etheridge, M.A., Wilkie, J.C., 1981. An assessment of dynamically recrystallized grainsize as a palaeopiezometer in quartz-bearing mylonite zones. Tectonophysics 78, 475–508.

Fiala, J., Fuchs, G., Wendt, J.I., 1995. Moldanubian Zone. Stratigraphy. In: Dallmeyer, R.D., Franke, W., Weber, K. (Eds.), Pre-Permian Geology of Central and Eastern Europe. Springer, pp. 418–422.

Franke, W., 1989a. Variscan plate tectonics in Central Europe – current ideas and open questions. Tectonophysics 169, 221–228.

Franke, W., 1989b. Tectonostratigraphic units in the Variscan belt of central Europe. In: Dallmeyer, R.D. (Ed.), Terranes in the Circum-Atlantic Palaeozoic Ocean, 230. Geological Society of America Special Paper, pp. 67–90.

Franke, W., 2000. The mid-European segment of the Variscides: tectonostratigraphic units, terrane boundaries and plate tectonic evolution. In: Franke, W., Haak, V., Oncken, O., Tanner, D. (Eds.), Orogenic Processes: Quantification and Modelling in the Variscan Belt. Geological Society of London Special Publications, vol. 179, pp. 35–61.

Frentzel, A., 1911. Das Passauer Granitmassiv. Geognostische Jahrhefte 24, 105–192.

Freudenberger, W., 1996. Deckgebirge nördlich der Donau. In: Bayerisches Geologisches Landesamt, Erläuterungen zur Geologischen Karte von Bayern 1:500 000, fourth ed. München, pp. 259–265.

Friedl, G., von Quadt, A., Ochsner, A., Finger, F., 1993. Timing of the Variscan orogeny in the Southern Bohemian Massif (NE-Austria) deduced from new U-Pb zircon and monazite dating. Terra Abstracts, Abstr. Suppl. 1, 5, 235–236.

Fuchs, G., 1976. Zur Entwicklung der Böhmischen Masse. Jahrbuch der Geologischen Bundesanstalt 119, 45–61.

Fuchs, G., 1986. Zur Diskussion um den Deckenbau der Böhmischen Masse. Jahrbuch der Geologischen Bundesanstalt 129, 41–49.

Galadí-Enríquez, E., in press. Geologische Karte von Bayern 1:25 000, Erläuterungen zum Blatt Nr. 7246 Tittling. Bayerisches Geologisches Landesamt, München.

Galadí-Enríquez, E., Zulauf, G., Heidelbach, F., Dörr, W., Rohrmüller, J., 2005. Variscan dyke emplacement and sinistral strike slip in the Bavarian Forest (SE Germany): constraints on the evolution of the Bavarian Pfahl shear zone. Schriftenreihe der Deutschen Gesellschaft für Geowissenschaften 39, 111–112.

Gapais, D., Barbarin, B., 1986. Quartz fabric transition in a cooling syntectonic granite (Hermitage Massif, France). Tectonophysics 125, 357–370.

Gower, R.J.W., Simpson, C., 1992. Phase boundary mobility in naturally deformed, high-grade quartzofeldspathic rocks: evidence for diffusional creep. Journal of Structural Geology 14, 301–314.

Grant, J.A., 1986. The isocon diagram – a simple solution to Gresens' equation for metasomatic alteration. Economic Geology 81, 1976–1982.

Grauert, B., Hänny, R., Soptrajanova, G., 1974. Geochronology of a polymetamorphic and anatectic gneiss region: the Moldanubicum of the area Lam-Deggendorf, Eastern Bavaria, Germany. Contributions to Mineralogy and Petrology 45, 37–63.

Hanmer, S., Passchier, C., 1991. Shear-sense indicators: a review. Geological Survey of Canada Paper 90, 1–71.

Hoffmann, R., 1962. Die Tektonik des Bayerischen Pfahls. Geologische Rundschau 52, 332–346.

Jessell, M.W., Lister, G.S., 1990. A simulation of the temperature dependence of quartz fabrics. In: Knipe, R.J., Rutter, E.H. (Eds.), Deformation Mechanisms, Rheology and Tectonics. Geological Society Special Publication, vol. 54, pp. 353–362.

Kalt, A., Corfu, F., Wijbrans, J.R., 2000. Time calibration of a P-T path from a Variscan high-temperature low-pressure metamorphic complex (Bayerische Wald, Germany), and the detection of inherited monazite. Contributions to Mineralogy and Petrology 138, 143–163.

Koch, P.S., 1983. Rheology and microstructures of experimentally deformed quartz aggregates. PhD thesis, University of California.

Kruhl, J.H., 1996. Prism- and basal-plane parallel subgrain boundaries in quartz: a microstructural geothermobarometer. Journal of Metamorphic Geology 14, 581–589.

Law, R.D., 1990. Crystallographic fabrics: a selective review of their applications to research in structural geology. In: Knipe, R.J., Rutter, E.H. (Eds.), Deformation Mechanisms, Rheology and Tectonics. Geological Society Special Publication, vol. 54, pp. 335–352.

Lister, G.S., Snoke, A.W., 1984. S–C mylonites. Journal of Structural Geology 6, 617–638.

Mainprice, D., Bouchez, J.L., Blumenfeld, P., Tubia, J.M., 1986. Dominant *c* slip in naturally deformed quartz: implications for dramatic plastic softening at high temperature. Geology 14, 819–822.

Masberg, H.P., Hoffer, E., Hoernes, S., 1992. Microfabrics indicating granulite-facies metamorphism in the low-pressure central Damara Orogen, Namibia. Precambrian Research 55, 243–257.

Masch, L., Cetin, B., 1991. Gefüge, Deformationsmechanismen und Kinematik in ausgewählten Hochtemperatur-Mylonitzonen im Moldanubikum des Bayerischen Waldes. Geologica Bavarica 96, 7–27.

Matte, P., 1986. Tectonics and plate tectonics model for the Variscan belt of Europe. Tectonophysics 126, 329–374.

Matte, P., 1991. Accretionary history and crustal evolution of the Variscan belt in Western Europe. Tectonophysics 196, 309–337.

Matte, P., Maluski, H., Rajlich, P., Franke, W., 1990. Terrane boundaries in the Bohemian Massif: result of large-scale Variscan shearing. Tectonophysics 177, 151–170.

Mattern, F., 1995. Late Carboniferous to early Triassic shear sense reversals at strike-slip faults in eastern Bavaria. Zentralblatt für Geologie und Paläontologie Teil I 1993, 1471–1490.

Mercier, J.C.C., Anderson, D.A., Carter, N.L., 1977. Stress in the lithosphere: inferences from steady state flow of rocks. Pure and Applied Geophysics 115, 199–226.

Ord, A., Christie, J.M., 1984. Flow stresses from microstructures in mylonitic quartzites of the Moine Thrust Zone, Assynt area, Scotland. Journal of Structural Geology 6, 639–654.

Peach, C.J., Lisle, R.J., 1979. A FORTRAN IV program for the analysis of tectonic strain using deformed elliptical markers. Computers and Geosciences 5, 325–334.

Prior, D.J., Boyle, A.P., Brenker, F., Cheadle, M.C., Day, A., López, G., Peruzzo, L., Potts, G.J., Reddy, S., Spiess, R., Timms, N.E., Trimby, P., Wheeler, J., Zetterström, L., 1999. The application of electron backscatter diffraction and orientation contrast imaging in the SEM to textural problems in rocks. American Mineralogist 84, 1741–1759.

Propach, G., Baumann, A., Schulz-Schmalschläger, M., Grauert, B., 2000. Zircon and monazite U-Pb ages of Variscan granitoid rocks and gneisses in the Moldanubian zone of eastern Bavaria, Germany. Neues Jahrbuch für Geologie und Paläontologie Monatshefte 6, 345–377.

Ramsay, J.G., Graham, R.H., 1970. Strain variations in shear belts. Canadian Journal of Earth Sciences 7, 786–813.

Ramsay, J.G., Huber, M.I., 1983. The Techniques of Modern Structural Geology. In: Strain Analysis, Volume 1. Academic Press, London.

Sanderson, D.J., Marchini, W.R.D., 1984. Transpression. Journal of Structural Geology 6, 449–458.

Scheuvens, D., Zulauf, G., 2000. Exhumation, strain localization, and emplacement of granitoids along the western part of the Central Bohemian shear zone (Bohemian Massif). International Journal of Earth Sciences 89, 617–630.

Schmid, S.W., Casey, M., 1986. Complete fabric analysis of some commonly observed quartz *c*-axis patterns. Geophysical Monograph 36, 263–286.

Siebel, W., Blaha, U., Chen, F., Rohrmüller, J., 2005. Geochronology and geochemistry of a dyke-host rock association and implications for the formation of the Bavarian Pfahl shear zone, Bohemian Massif. International Journal of Earth Sciences 94, 8–23.

Simpson, C., Schmid, S.M., 1983. An evaluation of criteria to deduce the sense of movement in sheared rocks. Geological Society of America Bulletin 94, 1288.

Stipp, M., Stünitz, H., Heilbronner, R., Schmid, S.M., 2002. The eastern Tonale fault zone: a "natural laboratory" for crystal plastic deformation of quartz over a temperature range from 250 to 700 °C. Journal of Structural Geology 24, 1861–1884.

Stipp, M., Tullis, J., 2003. The recrystallized grain size piezometer for quartz. Geophysical Research Letters 30 (21), 2088, doi:10.1029/2003GL018444.

Suess, F.E., 1903. Bau und Bild der Böhmischen Masse. In: Diener, C., Hoernes, R., Suess, F.E., Uhlig, V. (Eds.), Bau und Bild Österreichs. Temsky-Freytag, Wien.

Teipel, U., Eichhorn, R., Loth, G., Rohrmüller, J., Höll, R., Kennedy, A., 2004. U-Pb SHRIMP and Nd isotopic data from the western Bohemian Massif (Bayerischer Wald, Germany): implications for Upper Vendian and Lower Ordovician magmatism. International Journal of Earth Sciences 93, 782–801.

Tikoff, B., Fossen, H., 1999. Three-dimensional reference deformations and strain facies. Journal of Structural Geology 21, 1497–1512.

Tullis, J., 1983. Deformation of feldspars. In: Ribbe, P.H. (Ed.), Feldspar Mineralogy. Reviews in Mineralogy, 2. Mineralogical Society of America, pp. 297–323.

Tullis, J., Yund, R.A., 1977. Experimental deformation of dry Westerly granite. Journal of Geophysical Research 82, 5705–5718.

Twiss, R.J., 1977. Theory and applicability of a recrystallized grain size piezometer. Pure and Applied Geophysics 115, 227–244.

Twiss, R.J., 1980. Static theory of size variation with stress for subgrains and dynamically recrystallized grains. US Geological Survey, Open File Report 80-625, pp. 665–683.

Unzog, W., 1990. Beispiele von Strainanalysen in Kristallingebieten. TSK III, 3. Symposium für Tektonik, Strukturgeologie, Kristallingeologie. Graz, 19–21 April 1990, pp. 265–266.

Wallbrecher, E., Brandmayr, M., Handler, R., 1990. Kinematische Untersuchungen an Blattverschiebungszonen in der südlichen Böhmischen Masse. Österreichische Beiträge zu Meteorologie und Geophysik 3, 97–120.

Watson, E.B., Harrison, T.M., 1983. Zircon saturation revisited: temperature and composition effects in a variety of crustal magma types. Earth and Planetary Science Letters 64, 295–304.

White, S.H., 1979. Paleostress estimates in the Moine Thrust zone. Nature 280, 222–223.

Wimmenauer, W., Bryhni, I., 2002. Towards a unified nomenclature in metamorphic petrology: migmatites and related rocks. A proposal on behalf of the IUGS Subcommission on the Systematics of Metamorphic Rocks. Web version of 31 July 2002, http://www.bgs.ac.uk/scmr/docs/paper_6/scmr_mig.pdf.

Zulauf, G., Dörr, W., Fiala, J., Kotková, J., Maluski, H., Valverde-Vaquero, P., 2002. Evidence for high-temperature diffusional creep preserved by rapid cooling of lower crust (North Bohemian shear zone, Czech Republic). Terra Nova 14, 343–354.